The Astrophysical Journal Letters, 708:L84–L88, 2010 January 10 doi:10.1088/2041-8205/708/2/L84

AGILE DETECTION OF DELAYED GAMMA-RAY EMISSION FROM THE SHORT GAMMA-RAY BURST GRB 090510

A. Giuliani[1], F. Fuschino[2], G. Vianello[1], M. Marisaldi[2], S. Mereghetti[1], M. Tavani[3,4], S. Cutini[5], G. Barbiellini[6], F. Longo[6], E. Moretti[6], M. Feroci[3], E. Del Monte[3], A. Argan[3], A. Bulgarelli[2], P. Caraveo[1], P. W. Cattaneo[7], A. W. Chen[1,8], T. Contessi[1,2], F. D'Ammando[3,4], E. Costa[3], G. De Paris[3], G. Di Cocco[2], I. Donnarumma[3], Y. Evangelista[3], A. Ferrari[8,9], M. Fiorini[1], M. Galli[10], F. Gianotti[2], C. Labanti[2], I. Lapshov[3], F. Lazzarotto[3], P. Lipari[11], A. Morselli[12], L. Pacciani[3], A. Pellizzoni[13], F. Perotti[1], G. Piano[3,4,12], P. Picozza[4,12], M. Pilia[14], G. Pucella[15], M. Prest[14], M. Rapisarda[15], A. Rappoldi[7], A. Rubini[3], S. Sabatini[4], E. Scalise[3], E. Striani[3,4,12], P. Soffitta[3], M. Trifoglio[2], A. Trois[3], E. Vallazza[6], S. Vercellone[16], V. Vittorini[3,4], A. Zambra[1], D. Zanello[11], C. Pittori[5], F. Verrecchia[5], P. Santolamazza[5], P. Giommi[5], S. Colafrancesco[5], L. A. Antonelli[17], and L. Salotti[18]

[1] INAF/IASF-Milano, I-20133 Milano, Italy
[2] INAF/IASF-Bologna, I-40129 Bologna, Italy
[3] INAF/IASF-Roma, I-00133 Roma, Italy
[4] Dip. di Fisica, Univ. Tor Vergata, I-00133 Roma, Italy
[5] ASI Science Data Center, I-00044 Frascati (Roma), Italy
[6] Dip. Fisica and INFN Trieste, I-34127 Trieste, Italy
[7] INFN-Pavia, I-27100 Pavia, Italy
[8] CIFS-Torino, I-10133 Torino, Italy
[9] Dip. Fisica, Universitá di Torino, Turin, Italy
[10] ENEA-Bologna, I-40129 Bologna, Italy
[11] INFN-Roma La Sapienza, I-00185 Roma, Italy
[12] INFN Roma Tor Vergata, I-00133 Roma, Italy
[13] INAF-Osservatorio Astronomico di Cagliari, localita' Poggio dei Pini, strada 54, I-09012 Capoterra, Italy
[14] Dip. di Fisica, Univ. dell'Insubria, I-22100 Como, Italy
[15] ENEA Frascati, I-00044 Frascati (Roma), Italy
[16] INAF-IFC, Palermo, Italy
[17] INAF-Osservatorio Astron. di Roma, Monte Porzio Catone, Italy
[18] Agenzia Spaziale Italiana, I-00198 Roma, Italy
Received 2009 August 4; accepted 2009 September 11; published 2009 December 18

ABSTRACT

Short gamma-ray bursts (GRBs), typically lasting less than 2 s, are a special class of GRBs of great interest. We report the detection by the *AGILE* satellite of the short GRB 090510 which shows two clearly distinct emission phases: a prompt phase lasting ∼200 ms and a second phase lasting tens of seconds. The prompt phase is relatively intense in the 0.3–10 MeV range with a spectrum characterized by a large peak/cutoff energy near 3 MeV; in this phase, no significant high-energy gamma-ray emission is detected. At the end of the prompt phase, intense gamma-ray emission above 30 MeV is detected showing a power-law time decay of the flux of the type $t^{-1.3}$ and a broadband spectrum remarkably different from that of the prompt phase. It extends from sub-MeV to hundreds of MeV energies with a photon index $\alpha \simeq 1.5$. GRB 090510 provides the first case of a short GRB with delayed gamma-ray emission. We present the timing and spectral data of GRB 090510 and briefly discuss its remarkable properties within the current models of gamma-ray emission of short GRBs.

Key words: gamma rays: bursts

1. INTRODUCTION

Gamma-ray bursts (GRBs) are the most energetic explosions in our universe but only a few bursts were detected at gamma-ray energies above 100 MeV. The *EGRET* instrument on board the *Compton Gamma Ray Observatory* during its six-year lifetime detected five GRBs above 100 MeV Dingus (2001). Today, the currently operating *AGILE* and *Fermi* satellites have doubled the sample of GRBs detected at these energies (e.g., Giuliani et al. 2008; McEnery et al. 2008; Abdo et al. 2009). However, the great majority of GRBs with detected photons above 100 MeV are long bursts with typical durations above 2 s: they are possibly associated with stellar explosions of massive stars. Much less is known about the high-energy proprieties of *short* GRBs that show durations below 2 s. These short events are usually hard compared to the average properties of GRBs and are believed to be associated with the coalescence of neutron-star binaries (but see Zhang et al. 2009 for a more thorough discussion of the GRB classification and possible origin of the different classes). It is then very important to establish the gamma-ray properties of short GRBs. Before the advent of *AGILE* and *Fermi* no short-GRB was detected above a few MeV. The first short-GRB detection in the gamma-ray energy band was by *Fermi*: GRB 081024B (lasting about 0.8 s in the MeV range) was detected up to 3 GeV within the first 5 s after trigger (Omodei et al. 2008; Connaughton et al. 2008). We report here the *AGILE* detection of GRB 090510, the second short-GRB detected above 100 MeV.

The Italian *AGILE* satellite for gamma-ray astronomy has been operating since 2007 April (Tavani et al. 2009). The Gamma-Ray Imaging Detector (GRID; Barbiellini et al. 2002) on board *AGILE* covers one fifth of the sky in the 30 MeV–30 GeV energy range. This large field of view, together with a gamma-ray detection deadtime of order of ∼100 μs, makes it particularly suited for the observation of GRBs. The GRID high-energy data are complemented by those of other detectors on board the satellite, which operate in different energy ranges.

Super-*AGILE* provides GRB localizations, light curves, and spectra in the 18–60 keV range (Feroci et al. 2009, 2007; Del Monte et al. 2008). The Mini-Calorimeter (MCAL), besides being used as part of the GRID, can be used to autonomously detect and study GRBs in the 0.35–100 MeV range with excellent timing (Labanti et al. 2009; Marisaldi et al. 2008). Finally, GRB light curves in the hard X-ray band can be obtained also from the GRID anti coincidence scintillator panels (Perotti et al. 2006).

2. GRB 090510

The GRB 090510 was discovered and precisely localized by the *Swift* satellite (Gehrels et al. 2004) with coordinates (J2000) R.A. $= 22^{\rm h}14^{\rm m}12\overset{\rm s}{.}47$, decl. $= -26^\circ35'00\overset{''}{.}4$ (Hoversten et al. 2009). This burst was quite bright, with peak flux $\sim$10 ph cm^{-2} s^{-1} in the energy band 15–150 keV Ukwatta et al. (2009), and was independently detected also by Konus-Wind Golenetskii et al. (2009), Suzaku-WAM Ohmori et al. (2009), and *Fermi*-GBM Guiriec et al. (2009). The main emission lasts about 0.2 s with a multi-peak structure. Follow-up observations of the optical transient of GRB 090510 led to the determination of the redshift $z = 0.903 \pm 0.003$ (Rau et al. 2009).

This GRB occurred at the border of the standard *AGILE*-GRID field of view, at an off-axis angle of 61°. At this large off-axis angle, the *AGILE*-GRID effective area is $\sim$100 cm^2 for photon energies above 25 MeV. A quick look analysis of the GRID data showed an excess of photons above 30 MeV consistent with the direction of GRB 090510 Longo et al. (2009). GRB 090510 was also clearly detected in the 0.3–10 MeV energy range with the *AGILE*-MCAL, while it was not detected by Super-*AGILE*, owing to its large off-axis position. Emission above a few tens of MeV was also detected by the *Fermi*-LAT instrument Ohno et al. (2009).

3. *AGILE* TIMING AND SPECTRAL DATA

In the following, we refer all the times to T_0 corresponding to 00:23:00.5 UT of 2009 May 10. This corresponds to the time of the sharp initial increase of the GRB light curve in the MCAL detector. Based on the properties of the 0.3–10 MeV and $\geqslant$ 25 MeV emissions of GRB 090510 showing a clear dichotomy between the low- and high-energy gamma-ray emissions, we define two time intervals, Interval I from T_0 to $T_0 + 0.20$ s and Interval II from $T_0 + 0.20$ s to $T_0 + 1.20$ s (see Figure 2).

3.1. The Prompt Phase (Interval I)

The light curves of GRB 090510 obtained with the *AGILE*-MCAL in the 0.3–10 MeV are shown in Figure 1. As seen by MCAL, the burst has a duration (T90) of 184 ± 6 ms. During the T90 time interval MCAL recorded from the source more than 1000 counts above 330 keV, with an expected background of 60 counts over the same time interval. The peak flux of 18,000 counts s^{-1} in a 1 ms time bin was reached at time $T_0 + 0.024$ s. To date, this is the brightest short burst detected by MCAL in the GRID field of view. In the T90 time interval the observed emission can be divided into three main pulses, each of them showing millisecond time variability. At $T_0 - 0.55$ s a soft precursor lasting 15 ms is detected up to 700 keV, while at $T_0 + 0.29$ s another 15 ms peak is evident, with significant detection up to few MeV.

Most of the soft-gamma emission ($E \leqslant 10$ MeV) is concentrated in Interval I (between T_0 and $T_0 + 0.20$), where no

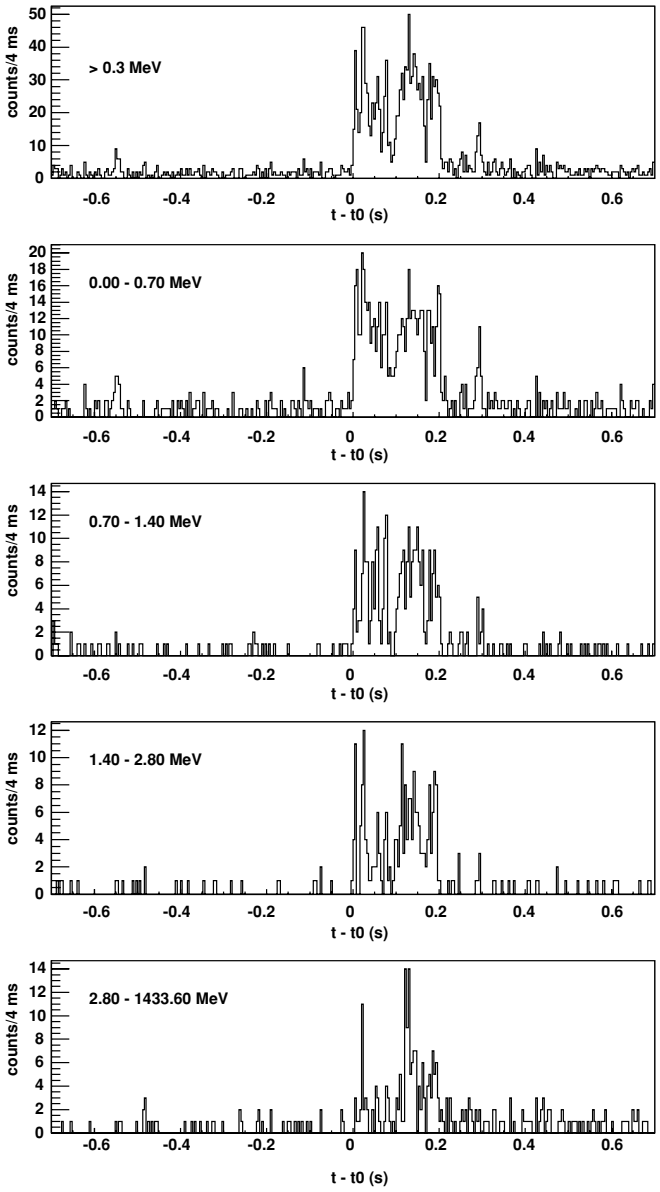

Figure 1. Light curve of GRB 090510 as detected by the *AGILE*-MCAL detector in different energy ranges. The time bin is 4 ms.

high-energy ($E \geqslant 25$ MeV) photons were detected. We derive the flux spectrum for the Interval I using the MCAL data. We find that the averaged MCAL spectrum is well described by a power-law model with exponential cutoff (reduced χ^2 of 0.8 for 23 dof). The photon index is $\alpha_1 = 0.65(-0.32 + 0.28)$ and the exponential cutoff energy is $E_c = 2.8(-0.6, +0.9)$ MeV. The integrated fluence (500 keV $\leqslant E \leqslant$ 10 MeV) during this interval is $F = 1.82(-0.41, +0.09) \times 10^{-5}$ erg cm^{-2}, all the errors for MCAL results reported throughout this paper are at the 90% confidence level. The GRID upper limit (at 3σ c.l.) is consistent with the extrapolation of this spectrum. The top panel of Figure 4 shows the Interval I spectrum. We also notice a substantial soft-to-hard spectral evolution during Interval I. If we define a hardness ratio as HR = (counts above 1 MeV)/(counts below 1 MeV), we obtain HR $\sim 0.6 \pm 0.1$ during the first peak (between T_0 and $T_0 + 0.12$) and HR $\sim 0.9 \pm 0.1$ during the second phase of Interval I (between $T_0 + 0.12$ and $T_0 + 0.20$).

A remarkable absence of gamma-ray events during Interval I is evident. In fact the first GRID events are detected only at the

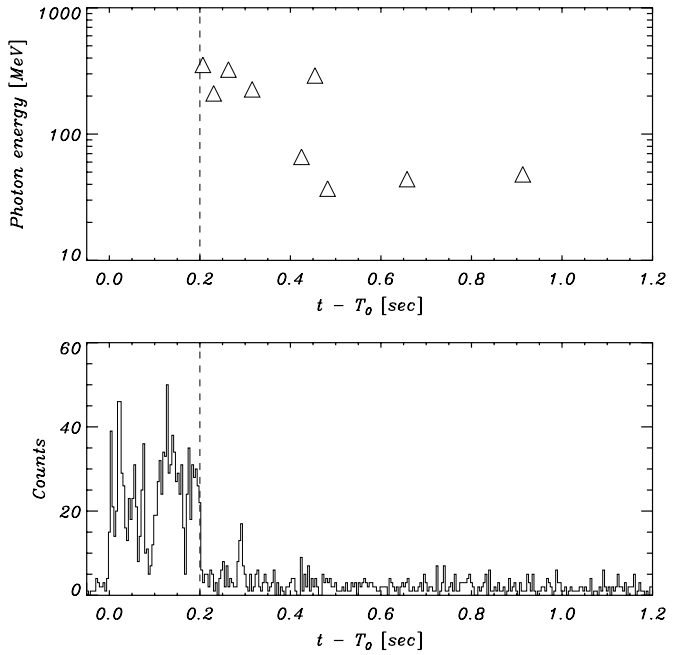

Figure 2. Top panel: energies vs. arrival time of the GRB photons detected by the *AGILE*-GRID in the 25 MeV–1 GeV energy range. Note the remarkable absence of gamma-ray events before $T_0 + 0.2$ s. Lower panel: 0.3–10 MeV light curve measured with the *AGILE*-MCAL detector. The dashed line separates Interval I from Interval II (see text).

end of the prompt emission. Note that a backward extrapolation to $t = T_0 + 0.01$ s of the GRID power-law light curve of Figure 3, discussed in the next section, would predict 28 photons in Interval I, while none was observed.

3.2. The Delayed Emission Phase: Interval II and Tail

The phase immediately following the sharp decay of the MeV flux at the end of Interval I shows a significant tail of MeV emission and the presence of a strong gamma-ray component above 30 MeV. We consider here the Interval II and a following tail of emission (lasting up to $T_0 + 10$ s).

During Interval II and tail, MCAL continues to detect significant emission in the 500 keV–10 MeV energy range with a spectrum significantly different from that of Interval I. Indeed, the derived power-law distribution has now photon index $\alpha_2 = -1.58(-0.11, +0.13)$. Significant emission is detected in the MCAL highest energy channels with no sign of cutoff. The Interval II fluence in the energy range 0.5–10 MeV range is $F_2 = 3.1(-0.7, +0.6) \times 10^{-6}$ erg cm^{-2}.

To search for emission above 30 MeV, we selected GRID gamma-ray events within 15° of the burst position. For this analysis we used all the GRID events with reliable direction and energy reconstructions, resulting in 15 events in the time interval from T_0 to $T_0 + 10$ s. The expected number of background events in this time interval is 1.4, implying that the GRB is detected above 30 MeV with a $\geqslant 5\sigma$ statistical significance.

The energy and arrival times of the GRID events are compared with the MCAL light curve in Figure 2. The GRID high-energy emission lasts for a few tens of seconds after the end of Interval I. The time evolution of the gamma-ray emission from GRB 090510 can be remarkably well described by a power-law decay, as shown in Figure 3(top panel). We model it with a function given by

$$F(t) \propto t^{-\delta} \quad \text{for} \quad t \geqslant T_0 + T_1 \qquad (1)$$

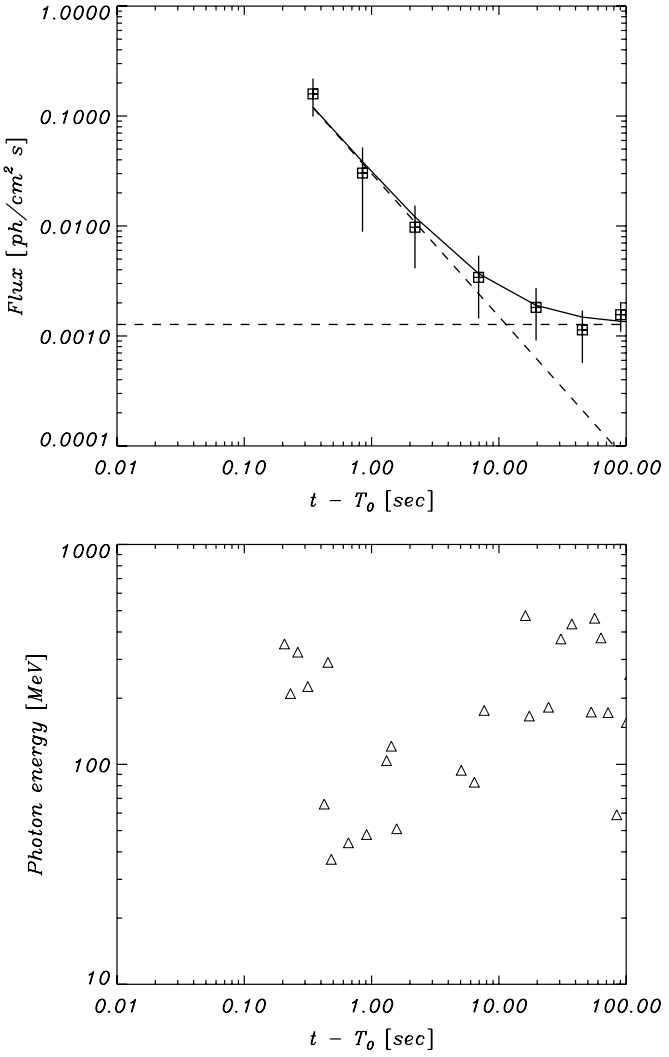

Figure 3. Top panel: *AGILE*-GRID gamma-ray light curve of GRB 090510 for photon events within a sky region of radius 15°. The inclined dashed line corresponds to a power-law time decay $t^{-\delta}$, with $\delta = 1.3$. The horizontal dashed line corresponds to the background flux measured in the 1000 s before the trigger. The solid line is the sum of the two components. Bottom panel: energies vs. arrival time of the GRB photons detected by the *AGILE*-GRID in the 25 MeV–1 GeV energy range. Note that after $T_0 + 10$ the detected counts are compatible with the background, as shown by the light curve in the top panel.

and $F(t) = 0$ for $t \leqslant T_0 + T_1$ and find that $T_1 = 0.2$ s, and $\delta = 1.30 \pm 0.15$ give the highest probability to reproduce the observed times of arrival. The corresponding power law is plotted in the Figure 3 (top panel). The background flux measured in the 1000 s before trigger is also shown in figure by the dashed horizontal line.

The energy distribution of the GRID photons during the time interval T_0 to $T_0 + 10$ s is consistent with a power-law spectrum of photon index $\alpha_3 = 1.4 \pm 0.4$ (1σ c.l.). For this spectrum the 25 MeV–500 MeV fluence in the same time interval is $(1.51 \pm 0.39) \times 10^{-1}$ ph cm^{-2}, corresponding to $F_3 = (2.90 \pm 0.75) \times 10^{-5}$ erg cm^{-2}.

To compute the GRID flux in Interval II, we assumed the same spectrum measured in the long "tail" between T_0 and $T_0 + 10$ (photon index -1.45 ± 0.07), and extrapolated the light curve with the best fit power-law decay. This gives $F_2' = 2.12 \times 10^{-5}$ erg cm^{-2} (25 MeV $\leqslant E \leqslant$ 500 MeV).

The MCAL + GRID spectrum of Interval II is shown in the bottom panel of Figure 4.

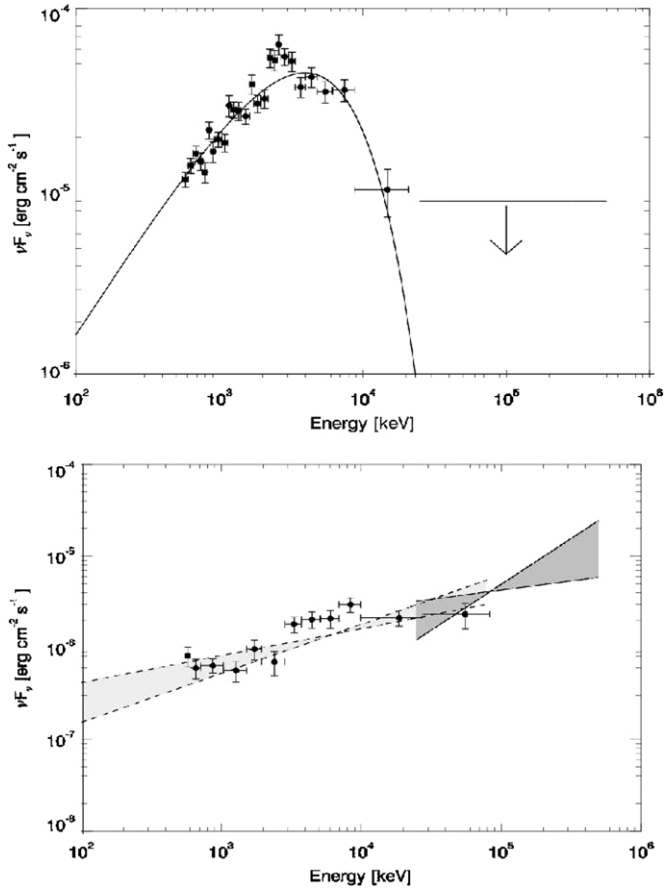

Figure 4. Top panel: gamma-ray power spectrum of GRB 090510 for Interval I. Bottom panel: gamma-ray power spectrum for Interval II.

4. DISCUSSION

Even though a theoretical investigation is beyond the scope of this paper, we can briefly emphasize a few relevant points here.

1. The broadband emission of GRB 090510 shows very distinct radiation phases during Interval I and the following delayed emission phase. Prompt gamma-rays above 30 MeV are absent during Interval I, but they constitute a crucial component during Interval II and the following tail. Remarkably, this is the first case of a delayed rise of the gamma-ray emission above 25 MeV detected in a short GRB. A similar behavior was shown by the long GRB 080916C Abdo et al. (2009). This fact suggests that the same process responsible for high-energy gamma-ray production takes place, in both long and short GRBs, independently from the central engine.
2. The prompt phase (Interval I) spectrum is peaked at $E_p = 3.78$ MeV. Comparing with other short GRBs (see Ghirlanda et al. 2009) we find that the E_p for GRB 090510 is the highest peak energy ever recorded for a short GRB (about 2.4σ greater than the mean value for short GRBs). Also the rest-frame peak energy ($E_p^{\rm rest} = 7.19(-1.54, +2.31)$ MeV) for GRB 090510 is greater than the $E_p^{\rm rest}$ for the other short GRBs with known redshift. The large value of $E_p^{\rm rest}$, combined with a quite usual value of the isotropic (comoving) energetics ($E_{\rm iso,1} = 3.91(-0.88, +1.91) \times 10^{52}$ erg in the whole energy range) and peak luminosity ($L_{\rm iso,1} = 7.74(-1.74, +3.79) \times 10^{53}$ erg s^{-1}), implies that GRB 090510 does not follow either the $E_p^{\rm rest} - E_{\rm iso}$ Amati relation (Amati et al. 2002) or the $E_p^{\rm rest}$–$L_{\rm iso}$ Yonetoku relation (Yonetoku et al. 2004). To our knowledge, this is the first short GRB that does not follow the Yonetoku relation. No significant emission is detected above 10 MeV, implying a rather strong constraint on any possible power-law emission above E_c ($\beta < -3.2$ at the 90% confidence level).
3. The prompt phase shows a significant soft-to-hard spectral evolution. As can be inferred from Figure 1 and from the MCAL hardness ratio calculations, the last peaks of Interval I are harder than the first peak.
4. Gamma-ray emission above 25 MeV extends in time for tens of seconds, i.e., well beyond the prompt phase duration, and shows a temporal behavior consistent with a power law of index $\delta = 1.30 \pm 0.15$.
5. The total isotropic energy of Interval II and tail is larger than that of Interval I: by summing the MCAL and GRID contributions to the emission, we obtain for the delayed phase $E_{\rm iso,2} = 4.8 \times 10^{52}$ erg.
6. The temporal index $\delta = 1.3$ is substantially different from that ($\delta' = 0.75$) subsequently measured by *Swift*-XRT between 80 and 1400 sec after trigger Grupe et al. (2009). This last phase can be attributed to an afterglow with spectral and temporal characteristics in agreement with expectations of fireball models (Zhang et al. 2006).

High-energy emission from GRB 090510 can have different physical origins at different phases. It is possible to evaluate a lower limit for the Lorentz factor of the emitting regions in Intervals I and II, on the basis of their spectral features and time-scale variability (Lithwich et al. 2001).

During Interval I the energy of the highest bin of the spectrum with significative detection is $E_{\rm max} = 20$ MeV. A physical scenario with the minimum Lorentz factor compatible with the data corresponds to a shell, optically thick for photons of energy greater than $m_e c^2$ (in the shell rest frame), moving with $\Gamma_I \geqslant (1+z)E_{\rm max}/m_e c^2 \simeq 80$. Otherwise, assuming that the emitting region is optically thin also for photons with energy greater than $m_e c^2$, a larger Lorentz factor is needed ($\Gamma_I \geqslant 150$) due to the fast variability during this phase, according to Equation (5) in Lithwich et al. (2001).

Emission during Interval II and following tail appears to be of a very different nature, and is clearly non-thermal. Several mechanisms can be at work, depending on the external environment and radiative conditions. Both synchrotron and inverse Compton (IC) emitting regions characterized by impulsively energized particles can be important contributors. The ultimate origin of fast and efficient acceleration is believed to be hydrodynamical shocks produced by expanding matter ejecta. Internal (IS) and external (ES) shocks can in principle contribute to both the synchrotron and IC emissions, and several models have been recently proposed to address the issue of the prompt versus the so-called delayed high-energy emission from GRBs. During Interval II the larger photon energy detected is $E_{\rm max} = 350$ MeV. The minimum Lorentz factor compatible with $E_{\rm max}$ is $\Gamma_{II} \geqslant 200$.

We postpone an investigation of these issues to forthcoming publications.

The *AGILE* Mission is funded by the Italian Space Agency (ASI) with scientific and programmatic participation by the Italian Institute of Astrophysics (INAF) and the Italian Institute of Nuclear Physics (INFN).

REFERENCES

Abdo, A. B., et al. 2009, Science, 323, 1688
Amati, L., et al. 2002, A&A, 390
Barbiellini, G., et al. 2002, Nucl. Instrum. Methods A, 490, 146
Connaughton, V., et al. 2008, GCN 8408
Del Monte, E., et al. 2008, A&A, 478, L5
Dingus, B. 2001, AIP Conf. Ser., Vol., 558, 383
Feroci, M., et al. 2007, Nucl. Instrum. Methods A, 581, 728
Feroci, M., et al. 2009, A&A, in press
Gehrels, N., et al. 2004, ApJ, 611, 1005
Ghirlanda, G., et al. 2009, A&A, 496, 585
Giuliani, A., et al. 2008, A&A, 491, L25
Golenetskii, S., et al. 2009, GCN 9344
Grupe, D., et al. 2009, GCN 9341
Guiriec, S., et al. 2009, GCN 9336
Hoversten, E. A., et al. 2009, GCN 9331
Labanti, C., et al. 2009, Nucl. Instrum. Methods A, 598, 470
Lithwich, Y., et al. 2001, ApJ, 555, 540
Longo, F., et al. 2009, GCN 9343
Marisaldi, M., et al. 2008, A&A, 490, 1151
McEnery, J., et al. 2008, GCN, 8684
Ohmori, N., et al. 2009, GCN 9335
Ohno, M., et al. 2009, GCN 9334
Omodei, N., et al. 2008, GCN 8407
Perotti, F., et al. 2006, Nucl. Instrum. Methods A, 556, 228
Rau, A., et al. 2009, GCN 9353
Tavani, M., et al. 2009, A&A, 502, 995
Ukwatta, T. N., et al. 2009, GCN 9337
Yonetoku, D., et al. 2004, ApJ, 609, 935
Zhang, B., et al. 2006, ApJ, 642, 354
Zhang, B., et al. 2009, ApJ, 703, 1696